

# Distinguishing a Slowly Accelerating Black Hole by Differential Time Delays of Images

Amjad Ashoorioon\* and Mohammad Bagher Jahani Poshteh†

*School of Physics, Institute for Research in Fundamental Sciences (IPM), P.O. Box 19395-5531, Tehran, Iran*

Robert B. Mann‡

*Department of Physics and Astronomy, University of Waterloo, Waterloo, Ontario, N2L 3G1, Canada*

*Perimeter Institute for Theoretical Physics, Waterloo, Ontario, N2L 2Y5, Canada*

Accelerating supermassive black holes, connected to cosmic strings, could contribute to structure formation and get captured by galaxies if their velocities are small. This would mean that the acceleration of these black holes is small too. Such a slow acceleration has no significant effect on the shadow of such supermassive black holes. We also show that, for slowly accelerating black holes, the angular position of images in the gravitational lensing effects do not change significantly. We propose a method to observe the acceleration of these black holes through the gravitational lensing. The method is based on the observation that differential time delays associated with the images are substantially different with respect to the case of non-accelerating black holes. This is in contrast with when the theory governing the strong gravitational field around the black hole is different from general relativity, where not only the differential time delays but the angular position of images would be different. We conclude that, if the observed angular position of images are compatible with the prediction of general relativity, a possible deviation in the differential time delays between the observed values and those predicted by general relativity, could be due to the acceleration of the black hole.

## I. INTRODUCTION

Some gauge theories allow the possibility of topological defects such as cosmic strings during first order phase transitions [1, 2] or at the end of brane inflation [3]. Cosmic strings could break or fray to produce pair of accelerating black holes [4, 5], which can also be produced in a background magnetic field [6–8], in de Sitter space [9–11], or on a cosmic string in background with both positive cosmological constant and magnetic field [12, 13]. Alternatively, there might be a network of cosmic strings, which later capture primordial black holes produced during their formation [14]. Such primordial black holes could form much later than the network of cosmic string formation, for example, from the reentry of fluctuations with large amplitudes generated during inflation [15, 16], or from the bubbles nucleated during inflation and collapse during the ensuing matter or radiation-dominated era [17, 18]. Such black holes would be accelerating due to the tension of the cosmic string.

Supermassive black holes connected to cosmic strings could reside in the centers of galaxies [14, 19]. The velocity of such black holes, however, should be small ( $\lesssim 100$  km/s), so that they can contribute to structure formation [14]. Therefore, the acceleration of these black holes must be very small. We take the acceleration so small that a ray of light, passing the black hole to the Earth, lies on the equatorial plane of the black hole dur-

ing its evolution. In this paper, we study gravitational lensing by such *slowly* accelerating black holes.

In the past few years accelerating black holes have attracted increasing attention due to their interesting thermodynamic properties [20–27], near horizon symmetries [28], and other features [29, 30]. Null geodesics around these black holes have also been studied [31, 32] and the shadow cast by them has been investigated in [33, 34].

Our aim is to study gravitational lensing by accelerating black holes. Studies of gravitational lensing in the strong field regime of Schwarzschild black holes traces back to the work of Darwin [35, 36]. In a lensing effect by a black hole, rays of light that are coming from a source behind the black hole are deflected near the black hole and turn toward an observer. The observer does not see the source at its real location, but rather sees images of it located apparently elsewhere. The image that is on the same side as the source is called the primary image. There is also an image on the opposite side which is called the secondary image.

On the other hand the light rays that pass very close the black hole would rotate around the hole before continuing their path to the observer. There is one set of an infinite number of such images in either side of the black hole [37]. These so-called relativistic images are very dim. Nonetheless if they are observed, they could be used to find very accurate values for the mass of the black hole and its distance to us [38].

Some features of gravitational lensing by accelerating black holes have been studied in [32] for a Carter observer. Here we study gravitational lensing as seen by a distant static observer, paying special attention to the time delays associated with the primary and secondary

---

\* amjad@ipm.ir

† jahani@ipm.ir

‡ rbmann@uwaterloo.ca

images. We take the supermassive black hole at the center of the M87 galaxy as the lens and take the acceleration to be sufficiently small so that the light ray passing the black hole stays on or near the equatorial plane during its transit from source to observer. For such small accelerations, the black hole can take part in structure formation [14]. The value of the acceleration parameter we assume for such a black hole is also consistent with the existing bounds on the abundance of primordial black holes too [14, 39], coming from the dynamical friction on compact objects [40]. We find, by studying the time delay, that even such a small acceleration could be observed.

The outline of our paper is as follows. In the next section we present the form of the metric that describes accelerating black holes and we are going to use throughout the paper. In Sec. III we review the basic equations of the gravitational lensing. In Sec. IV we investigate gravitational lensing by the black hole at the center of M87 galaxy. We assume this black hole to be non-rotating slowly accelerating as well as non-accelerating and compare the results of primary, secondary and relativistic images. We conclude our paper in Sec. V. The angular radius of the shadow of the (non-)accelerating M87\* is obtained in an appendix. We work in geometric units where  $G = c = 1$  and use mostly-positive signature for the spacetime metric.

## II. C METRIC IN SPHERICAL COORDINATES

Spacetime around uniformly accelerated black holes can be described by C metric [41]. An interesting form to represent the C metric has been introduced in [42],

$$ds^2 = \frac{1}{\alpha^2(x+y)^2} \times \left[ -F(y)d\tau^2 + \frac{dy^2}{F(y)} + \frac{dx^2}{G(x)} + G(x)d\phi^2 \right], \quad (1)$$

where

$$\begin{aligned} F(y) &= -(1-y^2)(1-2\alpha my), \\ G(x) &= (1-x^2)(1+2\alpha mx), \end{aligned} \quad (2)$$

and  $m$  is the mass parameter. The advantage of this form over the usual representation of C metric is that, here, the factorisable form of the structure functions  $F(y)$  and  $G(x)$  makes the roots trivial to write down. To keep the order of the roots, it is necessary to take  $0 < 2\alpha m < 1$ . One finds from Eq. (1) that  $x + y = 0$  corresponds to conformal infinity (see [42] for more features of this metric).

An issue related to the metric (1) is that it has no convenient limit as  $\alpha \rightarrow 0$ . To overcome this problem, the authors of [43] have used the transformation

$$x = \cos \theta, \quad y = \frac{1}{\alpha r}, \quad \tau = \alpha t, \quad (3)$$

to write C metric in the spherical-like coordinates

$$ds^2 = \frac{1}{(1 + \alpha r \cos \theta)^2} \times \left[ -Q(r)dt^2 + \frac{dr^2}{Q(r)} + \frac{r^2 d\theta^2}{P(\theta)} + P(\theta)r^2 \sin^2 \theta d\phi^2 \right], \quad (4)$$

where

$$\begin{aligned} Q(r) &= (1 - \alpha^2 r^2) \left( 1 - \frac{2m}{r} \right), \\ P(\theta) &= 1 + 2\alpha m \cos \theta. \end{aligned} \quad (5)$$

It is obvious that the above metric reduces to the Schwarzschild solution<sup>1</sup> for  $\alpha \rightarrow 0$ . The parameter  $\alpha$  has been interpreted as the acceleration of the black hole [43].

The Kretschmann curvature invariant obtained from the Riemann tensor  $R_{\mu\nu\gamma\delta}$ , for the metric (4), is

$$R_{\mu\nu\gamma\delta}R^{\mu\nu\gamma\delta} = 48m^2 \left( \frac{1}{r} + \alpha \cos \theta \right)^6 = 48m^2 \alpha^6 (x+y)^6, \quad (6)$$

which diverges at  $r = 0$ , indicating a physical singularity at this point. Note that Eq. (6) returns the Kretschmann scalar of Schwarzschild black holes in the  $\alpha \rightarrow 0$  limit. One finds that this curvature invariant is zero for  $m = 0$ , indicating a flat spacetime.

Eq. (6) shows that the spacetime is also flat for  $x+y \rightarrow 0$ , i.e. near conformal infinity. However, the curvature invariant does not vanish for  $r \rightarrow \infty$  unless  $\theta = \pi/2$ . We would like to study the lensing effects on the equatorial plane of accelerating black holes,  $\theta = \pi/2$ . On this plane, the line element (4) reduces to

$$ds^2 = -Qdt^2 + \frac{dr^2}{Q} + r^2 d\theta^2 + r^2 d\phi^2, \quad (7)$$

where  $Q(r)$  is given by (5).

## III. GRAVITATIONAL LENSING BY BLACK HOLES

In this section we review the basic equations that describe the gravitational lensing by black holes. In Fig. 1 we have schematically shown what happens in a lensing effect by a black hole. The light coming from the source would pass the black hole and deflect by the angle  $\hat{\alpha}$ . The observer would then see the image of the object with angular position  $\vartheta$ .

The equations governing the geodesics can be obtained using the Lagrangian

$$\mathcal{L} = \frac{1}{2} g_{\mu\nu} \dot{x}^\mu \dot{x}^\nu = \frac{1}{2} \left( -Q\dot{t}^2 + \frac{\dot{r}^2}{Q} + r^2 \dot{\phi}^2 \right), \quad (8)$$

<sup>1</sup> For the general case of charged rotating black holes, which also possess NUT charge parameter the metric has been obtained in [44].

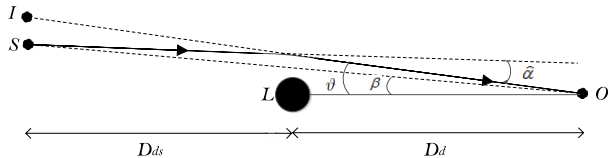


FIG. 1. *Deflection of light by the black hole:*  $S$ ,  $I$ ,  $O$ , and  $L$ , respectively stand for the source, image, observer, and the lens (black hole). The black hole is accelerating in a direction perpendicular to the plane of the figure and behind it there is an acceleration horizon at  $r = 1/\alpha$ , where  $\alpha$  is the acceleration, whose sign is not important in our approximation. The path of the light ray is on the equatorial plane of the black hole.  $\beta$  is the actual angular position of the source (with respect to the line of sight to the black hole). The black hole would bend the light ray by an angle  $\hat{\alpha}$  so that the observer sees the image on the angular position  $\vartheta$ .  $D_d$  and  $D_{ds}$  are the distance from lens to observer and from lens to the source, respectively.

where the dot denotes differentiation with respect to some affine parameter along the geodesic. We note that  $\dot{\theta} = 0$  as the particle is assumed to be on the equatorial plane. The constants of motion are

$$E = -\frac{\partial \mathcal{L}}{\partial \dot{t}} = Q\dot{t}, \quad L_z = -\frac{\partial \mathcal{L}}{\partial \dot{\phi}} = -r^2\dot{\phi}. \quad (9)$$

For the null geodesics  $\mathcal{L} = 0$  and we find from Eq. (8)

$$\frac{1}{Qr^2} \left( \frac{dr}{d\phi} \right)^2 = \frac{r^2 E^2}{Q L_z^2} - 1. \quad (10)$$

At the point of closest approach to the black hole,  $r = b$ , we have  $\frac{dr}{d\phi} = 0$ . Eq. (10) then yields  $E^2/L_z^2 = Q_b/b^2$ , where  $Q_b = Q(r = b)$ . Consequently Eq. (10) can be written as

$$\frac{d\phi}{dr} = \frac{1}{r\sqrt{\left(\frac{r}{b}\right)^2 Q_b - Q}}. \quad (11)$$

The deflection angle is then [45]<sup>2</sup>

$$\hat{\alpha}(b) = 2 \int_b^\infty \frac{dr}{r\sqrt{\left(\frac{r}{b}\right)^2 Q_b - Q}} - \pi, \quad (12)$$

where we have assumed that the distance from the black hole to the observer,  $D_d$ , and the distance from the

black hole to the source,  $D_{ds}$ , is much larger than  $b$ . We note that although the distances from the black hole to the observer/source are very large compared to the radius of the closest approach, they are still much smaller than the length scale set by the acceleration, i.e.  $1/\alpha \gg D_d, D_{ds} \gg b$ . In this regime, on the equatorial plane, the line element (7) is the appropriate one to work with.

Note that we have taken the direction of the acceleration to be perpendicular to the plane of the lens diagram, i.e. Fig. 1. If the acceleration has a component parallel to this plane, then the third component of the angular momentum is not a constant of motion and the geodesic equations cannot be integrated.

The time delay is the difference between the time it takes for the light to travel the physical path from the source to the observer and the time it takes to travel the path from the source to the observer when there is no black hole. To find the time delay we first rewrite the Lagrangian (8) for the null geodesics as

$$\frac{1}{Q^2} \left( \frac{dr}{dt} \right)^2 = 1 - \frac{Q}{r^2} \frac{L_z^2}{E^2}. \quad (13)$$

Since  $\frac{dr}{dt} = 0$  at  $r = b$ , we obtain

$$\frac{dt}{dr} = \frac{1}{Q\sqrt{1 - \left(\frac{b}{r}\right)^2 \frac{Q}{Q_b}}}. \quad (14)$$

The time delay can then be found by the integral

$$\tau(b) = \left[ \int_b^{r_s} dr + \int_b^{D_d} dr \right] \frac{1}{Q\sqrt{1 - \left(\frac{b}{r}\right)^2 \frac{Q}{Q_b}}} - D_s \sec \beta, \quad (15)$$

where  $\beta$  is the angular position of the source,  $D_s = D_d + D_{ds}$  is the distance from observer to the source and  $r_s = \sqrt{D_{ds}^2 + D_s^2 \tan^2 \beta}$ .

The image angular position,  $\vartheta$ , obeys the lens equation [46]

$$\tan \beta = \tan \vartheta - \mathcal{D} [\tan \vartheta + \tan(\hat{\alpha} - \vartheta)], \quad (16)$$

where  $\mathcal{D} = D_{ds}/D_s$ . The impact parameter is given by [47]

$$J = \frac{b}{\sqrt{Q_b}} = D_d \sin \vartheta. \quad (17)$$

Also the image magnification is

$$\mu = \left( \frac{\sin \beta \frac{d\beta}{d\vartheta}}{\sin \vartheta \frac{d\vartheta}{d\vartheta}} \right)^{-1}. \quad (18)$$

Differentiating Eq. (16) with respect to  $\vartheta$  we find

$$\sec^2 \beta \frac{d\beta}{d\vartheta} = \sec^2 \vartheta - \mathcal{D} \left[ \sec^2 \vartheta + \sec^2(\hat{\alpha} - \vartheta) \left( \frac{d\hat{\alpha}}{d\vartheta} - 1 \right) \right]. \quad (19)$$

<sup>2</sup> As can be seen from Eq. (5), the metric function  $Q$  changes sign at  $r = 1/\alpha$ . Because of the  $1/r$  factor in Eq. (12), the contribution of large  $r$  from  $\alpha^{-1}$  to infinity is very small in the integral of (12)—about one part in one million parts. Therefore we can safely integrate to infinity.

To find the derivative of the deflection angle with respect to  $\vartheta$ , we use  $\frac{d\hat{\alpha}}{d\vartheta} = \frac{d\hat{\alpha}}{db} \frac{db}{d\vartheta}$ . The factor  $\frac{db}{d\vartheta}$  can be found by using Eq. (17). The factor  $\frac{d\hat{\alpha}}{db}$  is a sort of tricky and has been found in [48] as

$$\frac{d\hat{\alpha}(b)}{db} = -2 \int_b^\infty \frac{1}{\sqrt{\mathcal{F}}} \frac{\partial}{\partial r} \left( \frac{1}{r} \frac{\partial \mathcal{F}}{\partial b} \frac{\partial r}{\partial \mathcal{F}} \right) dr, \quad (20)$$

where  $\mathcal{F} = \left(\frac{r}{b}\right)^2 Q_b - Q$ . The results which have been presented in this section will be used in the rest of the paper to study the gravitational lensing by accelerating black holes.

#### IV. GRAVITATIONAL LENSING BY M87\*

In this section we study the gravitational lensing by the black hole at the center of M87 galaxy. Since zero rotation is allowed by Event Horizon Telescope observation of M87\*, we take this black hole to be non-rotating [49]. We use numerical methods [37, 48] to investigate its gravitational lensing assuming this black hole is accelerating and compare image positions, magnifications and (differential) time delays to the case where it is non-accelerating.

The mass and distance of M87\* have been obtained by Event Horizon Telescope Collaboration as  $M_{\text{M87}^*} = 9.6 \times 10^{12} \text{ m} \equiv 6.5 \times 10^9 M_\odot$ ,  $D_d = 5.2 \times 10^{23} \text{ m}$  [50]. Whenever we consider an accelerating black hole, we take the acceleration  $\alpha$  to be small enough so that a light ray stays roughly on the equatorial plane throughout its pass from source to observer. Observation indicates that this is  $\alpha = 10^{-25} \text{ m}^{-1}$ , roughly the upper bound obtained by [14] from the development of a cosmic string network with black holes of such masses as beads in the network. It has also been assumed that the velocity of the black hole is small enough to contribute to structure formation and the relative abundance such black holes to the dark matter energy density is consistent with dynamical constraints coming from the disruption of binary stars or open star clusters,  $f_{\text{PBH}} \lesssim 10^{-3}$ , [40]. We also assume that the black hole is halfway between the source and the observer; therefore  $\mathcal{D} = 0.5$ .

The closer the light ray passes the black hole, the greater the deflection angle. In Fig. 2 we have plotted the deflection angle  $\hat{\alpha}$  as a function of the impact parameter  $b$  by using Eq. 12. We have taken the mass of the lens (black hole) to be equal the mass of M87\* and have assumed that the distance from the black hole to the observer/source is much larger than the impact parameter. We have also assumed that this black hole is slowly accelerating with  $\alpha = 10^{-25} \text{ m}^{-1}$ . The small value of the acceleration does not change the value of the deflection angle significantly. In fact, for a fixed value of the impact parameter, the deflection angle of non-accelerating black hole is greater than the deflection angle of accelerating black hole only by about 1 part in  $10^{13}$  parts. Since the deflection angle is in units of arcseconds, such deviations cannot be observed in the near future. Nonetheless, one

finds from Fig. 2 that the deflection angle decreases by increasing the impact parameter.

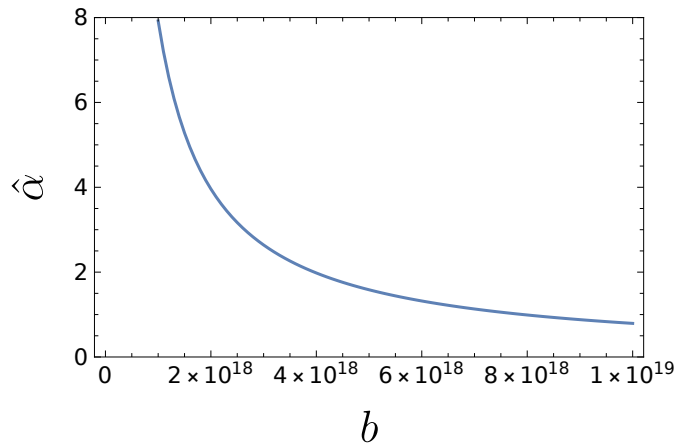


FIG. 2. Deflection angle as a function of impact parameter: The deflection angle  $\hat{\alpha}$  is in arcseconds and the impact parameter  $b$  is in meters. We have set  $M_{\text{M87}^*} = 9.6 \times 10^{12} \text{ m}$  and  $\alpha = 10^{-25} \text{ m}^{-1}$ .

#### A. Primary and secondary images

In Table I, by using eqs. (12), (16), (17), (18), and (20), we have computed image positions, deflection angles, impact parameters, and magnifications of primary and secondary images for different values of the source angular positions. The values presented in this table hold for both a non-accelerating and slowly accelerating M87\*. These quantities do not depend on the acceleration significantly. For a fixed value of the source angular position  $\beta$ , the impact parameter in the non-accelerating case is greater than that of the slowly accelerating case by only about 1 part in  $10^{13}$ . On the other hand, the (absolute value of) the image angular position is larger for the accelerating case by only about 1 part in  $10^{17}$ .

Therefore, it is impossible (at least by using the current and near future observational facilities) to tell if M87\* is non-accelerating or slowly accelerating by using the image positions produced from gravitational lensing. As we will show in Appendix A it is also impossible to tell if M87\* is non-accelerating or slowly accelerating by using its shadow. The (absolute value of) magnification of images are greater in the slowly accelerating case by about 1 part in  $10^{17}$  parts, as well.

One finds from Table I that the angular position of primary images increase with increasing the angular position of the source. However, the absolute value of the angular position of secondary images decrease with increasing the angular source position. Also, the absolute value of magnifications of primary and secondary images decrease with increasing the angular source position. This means that it would be more difficult to observe sources

with larger  $\beta$ . These results are also presented in Fig. 3.

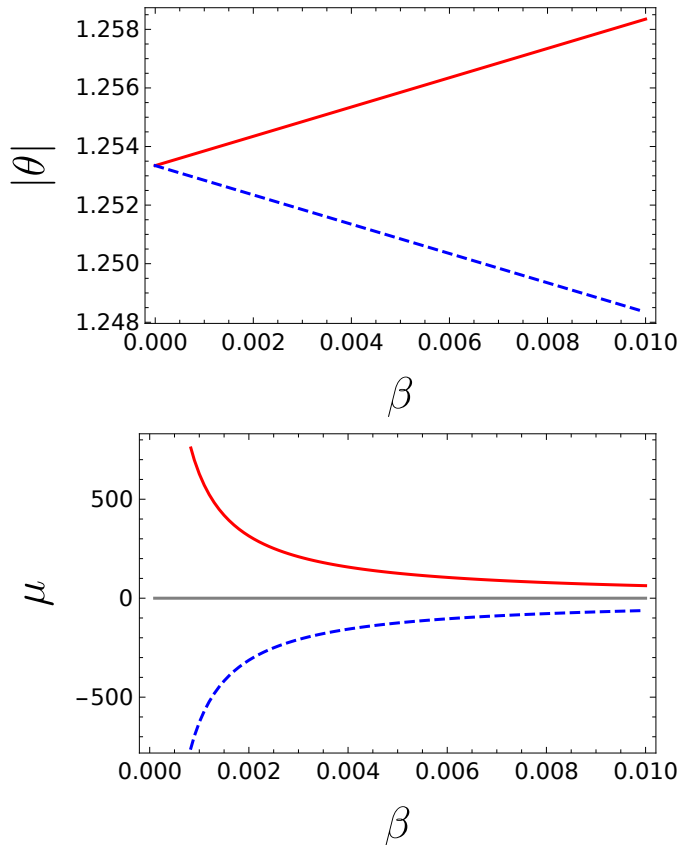


FIG. 3. *Image position and magnification of primary and secondary images:* (Top) Angular position of primary images  $\theta_p$  (red line) and the absolute value of angular position of secondary images  $|\theta_s|$  (dashed blue line) as a function of source angular position  $\beta$ . (Bottom) Magnification of primary (red line) and secondary (dashed blue line) images. Angles are in *arcseconds*. We have set  $M_{\text{M87}^*} = 9.6 \times 10^{12}$  m,  $D_d = 5.2 \times 10^{23}$  m,  $\mathcal{D} = 0.5$ , and  $\alpha = 10^{-25} \text{m}^{-1}$ .

In Table II, by using eq. (15), we have calculated the time delay of primary images due to lensing by M87\*. We presented the results for the case in which the black hole is non-accelerating and also for the case in which the black hole is accelerating with the acceleration  $\alpha = 10^{-25} \text{m}^{-1}$ . In both cases, the time delay of primary images decrease with increasing the angular source position (for the secondary images, however, we can show that the time delay increases by increasing  $\beta$ ). Quite strikingly, even this small acceleration increases the time delay by 6 orders of magnitude. This is notwithstanding that the deflection angles do not differ significantly if the black hole is accelerating. To understand this feature, recall from the metric function (5) that the acceleration makes important changes on the metric function only at large distances. The large distances do not have a significant contribution in the integral (12) due to the  $1/r$  factor. Therefore, the acceleration  $\alpha$  does not change the deflection angle significantly. However, the story is dif-

ferent when it comes to the time delay. The integrals of Eq. (15) do not have a  $1/r$  factor and the large distances have a significant contribution in the calculation of time delay. Hence, the acceleration would change the time delay significantly.

What is of observational importance is the differential time delay  $t_d = \tau_s - \tau_p$  (and  $\bar{t}_d$ ), which we provide in Table II (instead of explicit values of time delays of secondary images). In fact  $\tau_s$  and  $\tau_p$  cannot be observed, but if the source is pulsating every phase in its period would appear in the secondary image  $t_d$  second after it appears in the primary image. One finds that the differential time delay  $t_d$  increases with increasing the source angular position, as has been depicted in top panel of Fig. 4 as well.

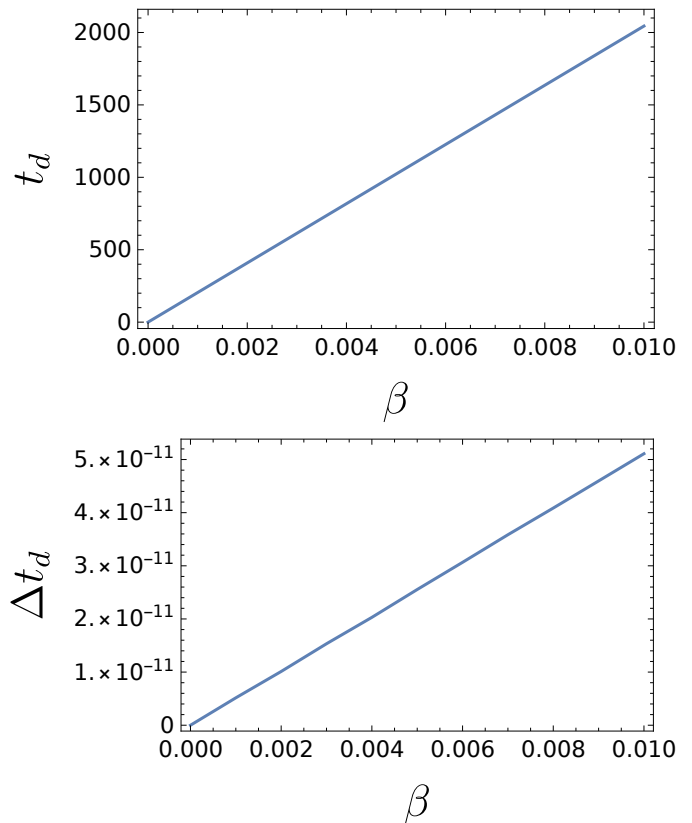


FIG. 4. *Differential time delay:* (Top) The differential time delay  $t_d = \tau_s - \tau_p$  of secondary and primary images as a function of source angular position for accelerating black hole. (Bottom) The difference between the differential time delay in non-accelerating and slowly accelerating cases,  $\Delta t_d = \bar{t}_d - t_d$ . Time delays are in units of *seconds* and  $\beta$  is in units of *arcseconds*. We have set  $M_{\text{M87}^*} = 9.6 \times 10^{12}$  m,  $D_d = 5.2 \times 10^{23}$  m,  $\mathcal{D} = 0.5$ , and  $\alpha = 10^{-25} \text{m}^{-1}$ .

It is interesting that, although the acceleration changes the values of  $\tau_p$  (and  $\tau_s$ ) significantly, the observable quantity  $t_d$  does not deviate from its non-accelerating counterpart  $\bar{t}_d$  that much. Still the difference is much larger than what one would naively expect from expand-

TABLE I. *Image positions, deflection angles, impact parameters, and magnifications of primary and secondary images due to lensing by M87\**: Angular positions  $\theta$ , bending angles  $\hat{\alpha}$ , impact parameters  $b$ , and magnifications  $\mu$  are given for different values of angular source position  $\beta$ . These results are the same in the non-accelerating and slowly accelerating cases. (a)  $p$  and  $s$  refer to primary and secondary images, respectively. (b) All angles are in *arcseconds* and the impact parameters are in *meters*. (c) We have used  $M_{M87^*} = 9.6 \times 10^{12}$  m,  $D_d = 5.2 \times 10^{23}$  m,  $\mathcal{D} = 0.5$ , and  $\alpha = 10^{-25} \text{m}^{-1}$ .

$\beta$	$\theta_p$	$\hat{\alpha}_p$	$b_p$	$\mu_p$	$\theta_s$	$\hat{\alpha}_s$	$b_s$	$\mu_s$
0	1.25334	2.50668	$3.20 \times 10^{18}$	$\times$	-1.25334	2.50668	$3.20 \times 10^{18}$	$\times$
0.1	1.30436	2.40872	$3.29 \times 10^{18}$	6.79185	-1.20436	2.60872	$3.04 \times 10^{18}$	-5.78173
0.5	1.52806	2.05611	$3.85 \times 10^{18}$	1.82812	-1.02805	3.05611	$2.59 \times 10^{18}$	-0.826954
1	1.84943	1.69886	$4.66 \times 10^{18}$	1.26694	-0.849483	3.69897	$2.14 \times 10^{18}$	-0.267388
2	2.60342	1.20683	$6.56 \times 10^{18}$	1.05575	-0.603448	5.20690	$1.51 \times 10^{18}$	-0.0567785
3	3.45471	0.909423	$8.71 \times 10^{18}$	1.01705	-0.454745	6.90949	$1.14 \times 10^{18}$	-0.0176322
4	4.36033	0.720660	$1.10 \times 10^{19}$	1.00676	-0.360286	8.72057	$9.08 \times 10^{17}$	-0.00687431

TABLE II. *Time delays of primary and secondary images due to lensing by M87\**: Time delays  $\tau$  are given for different values of angular source position  $\beta$ . Instead of the time delays of secondary images  $\tau_s$ , we present the differential time delay  $t_d = \tau_s - \tau_p$  which is of observational importance. (a) As in Table I. (b)  $\beta$  is in *arcseconds* and the (differential) time delays are in *seconds*. (c) As in Table I. (d) Barred quantities refer to values of the case that the black hole is not accelerating and  $\Delta t_d = \bar{t}_d - t_d$ .

$\beta$	$\tau_p$	$t_d$	$\bar{\tau}_p$	$\bar{t}_d$	$\Delta t_d$
0	$3.13186970 \times 10^{12}$	0	$1.62727362 \times 10^6$	0	0
0.1	$3.13186969 \times 10^{12}$	20445.4686829920	$1.61725037 \times 10^6$	20445.4686829935	$1.52795 \times 10^{-9}$
0.5	$3.13186965 \times 10^{12}$	102871.116191642	$1.58092945 \times 10^6$	102871.116191651	$8.42556 \times 10^{-9}$
1	$3.13186961 \times 10^{12}$	209681.897709557	$1.54280388 \times 10^6$	209681.897709578	$2.17115 \times 10^{-8}$
2	$3.13186955 \times 10^{12}$	448736.764965694	$1.48443381 \times 10^6$	448736.764965783	$8.89995 \times 10^{-8}$
3	$3.13186951 \times 10^{12}$	737888.423902370	$1.44178393 \times 10^6$	737888.423902647	$2.76603 \times 10^{-7}$
4	$3.13186948 \times 10^{12}$	1089214.16844197	$1.40880628 \times 10^6$	1089214.168442669	$7.01752 \times 10^{-7}$

ing the integrand in equation (15) to order  $\alpha^2$ <sup>3</sup>. In the last column of Table II we have presented the difference  $\Delta t_d = \bar{t}_d - t_d$ , which is a positive quantity; for a fixed value of angular source position, the differential time delay of secondary and primary images is larger if the black hole is not accelerating. The difference increases with increasing the angular source position as has also been shown in the bottom panel of Fig. 4.

These results imply that it is indeed feasible to observe if M87\* is accelerating or not. Thanks to the accuracy in time measurements, small changes  $\Delta t_d$  in the value of the differential time delay can be measured. We note that, although the distance to the source (and hence  $\mathcal{D}$ ) can be measured from its redshift [51], one cannot observe the angular source position  $\beta$ . What one sees are primary and secondary images of the source and, if the source has reliable variability, the differential time delay. Small

acceleration does not change the angular positions of primary and secondary images by an amount that could be observed. Therefore, we observe two images with the same positions whether the lens is slowly accelerating or not. From these images we can find angular source position  $\beta$  by using the top panel of Fig. 3. If the differential time delay  $\bar{t}_d$  corresponding to this  $\beta$  matches the observed value of the differential time delay then the black hole is non-accelerating. Conversely, if this  $\bar{t}_d$  does not match the observed value of the differential time delay then the black hole is slowly accelerating.

## B. Relativistic images

For small values of the impact parameter (with the same order of magnitude as the black hole radius), the light ray may rotate around the black hole before completing its path to the observer [37]. If the light ray circles the black hole once/twice the image hence produced is called the first/second order relativistic image (and higher order relativistic images if the light ray circles the black hole even more). These images are very dim [37] and very difficult to observe. But we can ask what in principle can learn we from them.

<sup>3</sup> If one expands the integrand in Eq. (15) for the time delay, and compute the coefficient of first correction to the Schwarzschild value, which is proportional to  $\alpha^2$ , it turns out to be large and compensates for the smallness of  $\alpha^2$ , even for small values of the acceleration parameters. Nonetheless, the value of the first order correction is not the same as the integral of the exact integrand as a function of  $\alpha$ , since one has to sum up all orders of  $\alpha$ .

In Table III we provide results for the first order relativistic images produced on the same side as the primary images as well as those produced on the same side as the secondary images for M87\*, considering both non-accelerating and slowly accelerating cases. As with the primary and secondary images, the angular positions of the first order relativistic images do not change significantly if the black hole is slowly accelerating. They are also nearly insensitive to the source angular position. The same is true for the impact parameter; it does not depend on  $\beta$  significantly and is insensitive to the (slow) acceleration of the black hole.

The absolute values of the magnifications of first order relativistic images on the same side of the primary image and on the same side of the secondary image are nearly the same. They are also nearly insensitive to whether the lens is slowly accelerating or non-accelerating. However, their absolute values decrease with increasing  $\beta$ . We note here that the first order relativistic images are highly demagnified, making the observation of these images very difficult.

In Table III, we have also presented the time delays of first order relativistic images on the same side of primary images. These time delays decrease with increasing the angular position of source. For the case in which the black hole is slowly accelerating, the time delay is 6 order of magnitude greater. However, the time delay itself is not an observable.

If the relativistic images could be observed, for pulsating sources one could measure the differential time delay. This quantity increases with increasing the angular source position. The difference between the differential time delay in the case of non-accelerating lens and slowly accelerating case,  $\Delta t_d$ , is very small (compared to the corresponding quantity for the primary and secondary images). Unlike the case of primary and secondary images, for the first order relativistic images  $\Delta t_d$  is negative, meaning that the differential time delays of first order relativistic images are lower if the black hole is non-accelerating. We also note that the absolute value of  $\Delta t_d$  increase with increasing the angular source position.

In Table IV we have presented the results of second order relativistic images. These images are dimmer than the first order relativistic images and the time delay associated to them is larger. On the other hand the differential time delay is lower for the second order relativistic images. These results are true whether the black hole is non-accelerating or slowly accelerating. Also, the absolute value of  $\Delta t_d$  is larger for second order relativistic images. The absolute value of  $\Delta t_d$  for first and second order relativistic images are plotted in Fig. 5.

For the relativistic images of first/second order, the images' positions are nearly fixed for different values of  $\beta$  and if the black hole is slowly accelerating or non-accelerating. However, both acceleration and  $\beta$  change the differential time delay. This means that by observing the differential time delay of first/second order relativistic images, one cannot tell if the black hole is slowly

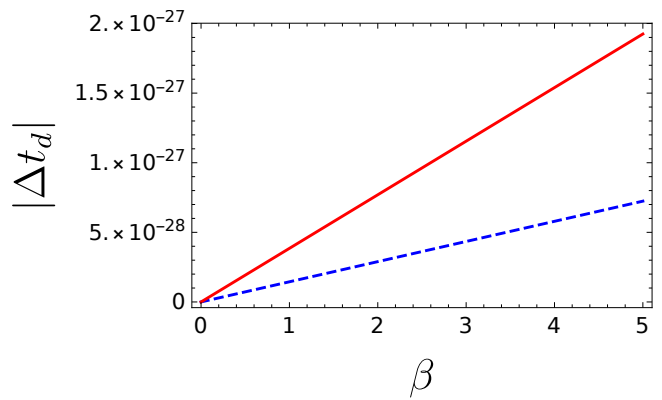


FIG. 5.  $\Delta t_d$  of first and second order relativistic images: The absolute value of  $\Delta t_d = \bar{t}_d - t_d$  of first order (dashed blue) and second order (red) relativistic images.  $\Delta t_d$  is in units of seconds and  $\beta$  is in units of microarcseconds. We have set  $M_{\text{M87}^*} = 9.6 \times 10^{12}$  m,  $D_d = 5.2 \times 10^{23}$  m,  $\mathcal{D} = 0.5$ , and  $\alpha = 10^{-25} \text{m}^{-1}$ .

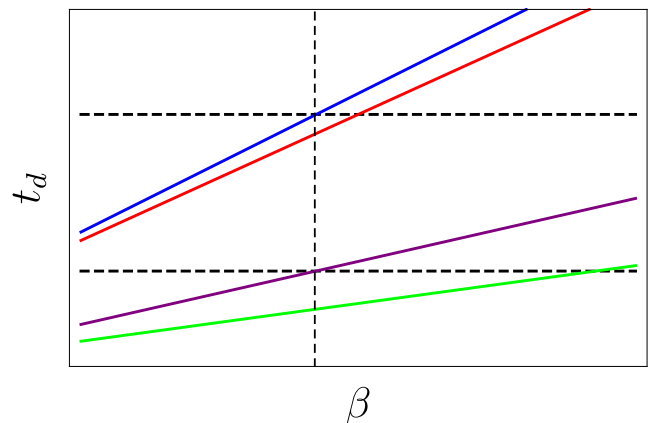


FIG. 6. Finding the acceleration and source position using relativistic images: The solid lines, respectively from top to bottom represent the differential time delay of first order relativistic images produced by accelerating black hole (blue line), that produced by non-accelerating black hole (red line), differential time delay of second order relativistic images produced by accelerating black hole (purple line), and that produced by non-accelerating black hole (green line). The slopes of these solid lines decrease from top to bottom. The separation between the lines are exaggerated in this schematic plot. The horizontal dashed lines indicate the observed values of first (upper line) and second (lower line) order relativistic images. The intersection points of the horizontal dashed lines with solid lines must have a common  $\beta$ .

accelerating; a change in the differential time delay might be due to a change in  $\beta$  and/or acceleration. Nevertheless measuring the time delay of both first and second order relativistic images can help.

From Tables III and IV and Fig. 5 we find that the plots of the differential time delay of the first/second order relativistic images in the case of slowly accelerating/non-accelerating black holes with respect to  $\beta$  all have differ-

TABLE III. *First order relativistic images due to lensing by M87\**: For different values of the angular source position  $\beta$ , we have presented the magnifications  $\mu$ , time delays  $\tau$ , and differential time delay  $t_d$  of first order relativistic images in both cases of non-accelerating and slowly accelerating lens. (a)  $1p$  ( $1s$ ) denotes the first order relativistic images on the same side of primary (secondary) image. (b)  $\beta$  is in *microarcseconds* ( $\mu as$ ) and the (differential) time delays are in *seconds*. (c) As in Table I. (d) As in Table II. In all the cases the impact parameter is  $b \simeq 3.38 \times 10^{13}$  m and the angular position of first order relativistic images are  $\theta_{1p} \simeq -\theta_{1s} \simeq 20.3991 \mu as$ .  $\mu_{1s} = -\mu_{1p}$  and are nearly insensitive to the acceleration but change with  $\beta$ .

$\beta$	$\mu_{1p}$	$\tau_{1p}$	$t_d$	$\bar{\tau}_{1p}$	$\bar{t}_d$	$\Delta t_d$
0	$\times$	$3.131871716800 \times 10^{12}$	0	$3.648305345949 \times 10^6$	0	0
1	$1.28 \times 10^{-10}$	$3.131871716800 \times 10^{12}$	$3.33 \times 10^{-6}$	$3.648305345947 \times 10^6$	$3.33 \times 10^{-6}$	$-1.45 \times 10^{-28}$
2	$6.42 \times 10^{-11}$	$3.131871716800 \times 10^{12}$	$6.65 \times 10^{-6}$	$3.648305345946 \times 10^6$	$6.65 \times 10^{-6}$	$-2.90 \times 10^{-28}$
3	$4.28 \times 10^{-11}$	$3.131871716800 \times 10^{12}$	$9.98 \times 10^{-6}$	$3.648305345944 \times 10^6$	$9.98 \times 10^{-6}$	$-4.34 \times 10^{-28}$
4	$3.21 \times 10^{-11}$	$3.131871716800 \times 10^{12}$	0.0000133	$3.648305345943 \times 10^6$	0.0000133	$-5.79 \times 10^{-28}$
5	$2.57 \times 10^{-11}$	$3.131871716800 \times 10^{12}$	0.0000166	$3.648305345942 \times 10^6$	0.0000166	$-7.24 \times 10^{-28}$
6	$2.14 \times 10^{-11}$	$3.131871716800 \times 10^{12}$	0.0000200	$3.648305345940 \times 10^6$	0.0000200	$-8.69 \times 10^{-28}$

TABLE IV. *Second order relativistic images due to lensing by M87\**: For different values of the angular source position  $\beta$ , we have presented the magnifications  $\mu$ , time delays  $\tau$ , and differential time delay  $t_d$  of second order relativistic images in both cases of non-accelerating and slowly accelerating lens. (a)  $2p$  ( $2s$ ) denotes the second order relativistic images on the same side of primary (secondary) image. (b)  $\beta$  is in *microarcseconds* ( $\mu as$ ) and the (differential) time delays are in *seconds*. (c) As in Table I. (d) As in Table II. In all the cases the impact parameter is  $b \simeq 2.97 \times 10^{13}$  m and the angular position of second order relativistic images are  $\theta_{2p} \simeq -\theta_{2s} \simeq 19.8116 \mu as$ .  $\mu_{2s} = -\mu_{2p}$  and are nearly insensitive to the acceleration but change with  $\beta$ .

$\beta$	$\mu_{1p}$	$\tau_{1p}$	$t_d$	$\bar{\tau}_{1p}$	$\bar{t}_d$	$\Delta t_d$
0	$\times$	$3.131872244317 \times 10^{12}$	0	$4.175822690080 \times 10^6$	0	0
1	$4.79 \times 10^{-12}$	$3.131872244317 \times 10^{12}$	$3.23 \times 10^{-6}$	$4.175822690078 \times 10^6$	$3.23 \times 10^{-6}$	$-3.85 \times 10^{-28}$
2	$2.40 \times 10^{-12}$	$3.131872244317 \times 10^{12}$	$6.46 \times 10^{-6}$	$4.175822690077 \times 10^6$	$6.46 \times 10^{-6}$	$-7.70 \times 10^{-28}$
3	$1.60 \times 10^{-12}$	$3.131872244317 \times 10^{12}$	$9.69 \times 10^{-6}$	$4.175822690075 \times 10^6$	$9.69 \times 10^{-6}$	$-1.15 \times 10^{-27}$
4	$1.20 \times 10^{-12}$	$3.131872244317 \times 10^{12}$	0.0000129	$4.175822690074 \times 10^6$	0.0000129	$-1.54 \times 10^{-27}$
5	$9.58 \times 10^{-13}$	$3.131872244317 \times 10^{12}$	0.0000162	$4.175822690073 \times 10^6$	0.0000162	$-1.92 \times 10^{-27}$
6	$7.99 \times 10^{-13}$	$3.131872244317 \times 10^{12}$	0.0000194	$4.175822690072 \times 10^6$	0.0000194	$-2.31 \times 10^{-27}$

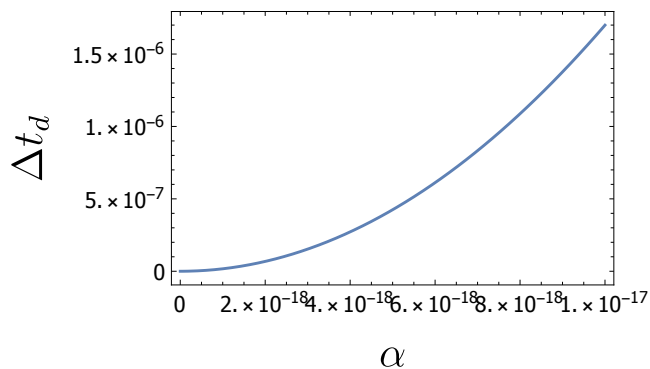


FIG. 7.  $\Delta t_d$  as a function of the acceleration: The difference between the differential time delay of accelerating and non-accelerating case.  $\Delta t_d$  is in units of *seconds* and  $\alpha$  is in units of  $m^{-1}$ . We have set  $M_{M87^*} = 9.6 \times 10^{12}$  m,  $D_d = \times 10^{15}$  m,  $D = 0.5$ , and  $\beta = 1$  *arcsecond*.

ent slopes. The situation has been schematically depicted in Fig. 6. Suppose we could measure the differential time delays of relativistic images. The observed value of the

differential time delay of first order relativistic images has been shown by the upper horizontal dashed line. This line crosses both  $t_d$  and  $\bar{t}_d$  plots of first order relativistic images. This means that the observed value can be due to lensing by either a non-accelerating black hole or a slowly accelerating black hole (suppose that we do not know  $\beta$ ). To break this degeneracy we need to measure the differential time delay of second order relativistic images. This has been depicted by the lower horizontal dashed line of Fig. 6. This line also crosses the plots for accelerating and non-accelerating black holes. Nevertheless this is the same source that causes the first and second order relativistic images. Therefore, the cross point of the lower horizontal line should be on the same vertical line as the cross point of the upper horizontal line. This way we can find out, not only if the black hole is accelerating or non-accelerating, but also the source angular position  $\beta$ .



TABLE V. *Lensing parameters for different values of the acceleration:* For different values of the acceleration  $\alpha$ , we have presented angular positions  $\theta$  of primary images and deflection angles  $\hat{\alpha}$ , magnifications  $\mu$ , time delays  $\tau$ , and differential time delay  $t_d = \tau_s - \tau_p$  associated to them. (a)  $p$  denotes the primary image. (b) All angles are in *arcseconds* (*as*),  $\alpha$  is in  $\text{m}^{-1}$ , and the (differential) time delays are in *seconds*. (c) We have used  $m = M_{\text{M87}^*} = 9.6 \times 10^{12}$  m,  $D_d = 10^{15}$  m,  $\mathcal{D} = 0.5$ , and  $\beta = 1 \text{ as}$ . In all the cases the impact parameter is  $b \simeq 1.43 \times 10^{14}$  m.

$\alpha$	$\theta_p$	$\hat{\alpha}_p$	$\mu_p$	$\tau_p$	$t_d$
0	31879.9967	63758.0408	13819.1819	367876	9.7208098
$2 \times 10^{-18}$	31879.9967	63758.0409	13819.1820	367884	9.7208097
$4 \times 10^{-18}$	31879.9969	63758.0413	13819.1821	367912	9.7208095
$6 \times 10^{-18}$	31879.9973	63758.0419	13819.1824	367958	9.7208092
$8 \times 10^{-18}$	31879.9977	63758.0429	13819.1827	368022	9.7208087
$10^{-17}$	31879.9983	63758.0441	13819.1832	368105	9.7208081

## V. CONCLUDING REMARKS

In gravitational lensing in the presence of an accelerating black hole, small changes accumulate over large distances from the source to the observer. We have shown that the differential time delay between the primary and secondary sources is considerably enhanced in the presence of an accelerating source. This may allow us to measure the acceleration of black holes, even if it is small. We also suggested a method for obtaining the exact angular position of the source, from the primary and secondary images, as well as from relativistic images.

We conclude that one can use gravitational lensing as a probe to measure the acceleration of a black hole that acts as a lens. We note that in the slow acceleration approximation that we are using the sign of the acceleration is not important.

## VI. ACKNOWLEDGMENTS

This project has received funding /support from the European Unions Horizon 2020 research and innovation programme under the Marie Skłodowska -Curie grant agreement No 860881-HIDDeN, and was supported in part by the Natural Sciences and Engineering Council of Canada. MBJP would like to acknowledge the support of Iran Science Elites Federation and the hospitality of the University of Guilan.

### Appendix A: Shadow of accelerating black hole

Shadows of accelerating black holes have been studied in [32–34]. It has been shown that for non-rotating accelerating black holes the shadow is circular and that the size of the shadow decrease with increasing the acceleration. Here we would like to find the shadow size of M87\* with acceleration  $\alpha = 10^{-25} \text{m}^{-1}$  and compare it to the shadow size in the non-accelerating case.

Angular radius of the shadow as seen by an observer at  $D_d$  is given by [52, 53]

$$\delta = \sin^{-1} \left( \sqrt{\frac{r_{ps}^2}{Q(r_{ps})} \frac{Q(D_d)}{D_d^2}} \right), \quad (\text{A1})$$

where  $r_{ps}$ , radius of the photon sphere, is the minimum of  $r^2/Q$  [53].

If we take M87\* to be a non-accelerating Schwarzschild black hole with mass  $M_{\text{M87}^*} = 9.6 \times 10^{12}$  m and distance  $D_d = 5.2 \times 10^{23}$  m from us, then the angular radius of its shadow would be  $\delta = 19.85 \mu\text{as}$ . However if M87\* is a non-rotating accelerating black hole, its shadow would appear to be a circle of radius  $\delta = 19.76 \mu\text{as}$ . We see that the shadow radius is less than  $0.1 \mu\text{as}$  smaller if M87\* is accelerating with  $\alpha = 10^{-25} \text{m}^{-1}$ . This is much lower than the resolution of today’s observational facilities such as Event Horizon Telescope [54, 55]. Therefore the current observations of the shadow cannot tell if M87\* is non-accelerating or slowly accelerating — not event they can say if M87\* is rotating or not [56]. Therefore, from theoretical point of view, gravitational lensing is a better probe to find out if M87\* is accelerating.

### Appendix B: Dependence on acceleration

To better understand the dependence of the lensing parameters on the acceleration, in this appendix we study different (and larger) values of  $\alpha$ . We consider a non-rotating black hole of the same mass as M87\*  $m = M_{\text{M87}^*} = 9.6 \times 10^{12}$  m but at a closer distance  $D_d = 10^{15}$  m. Since the black hole is at a closer distance, the deflection angle and the magnification is much larger than the case we have studied in Sec. IV. This can be seen in Table V.

In Table V we see that the differential time delay decrease by increasing the acceleration. This point is also obvious from Fig. 7 where we have plotted the difference between the differential time delay of in non-accelerating case and accelerating case,  $\Delta t_d = \bar{t}_d - t_d$ .

- 
- [1] T. W. B. Kibble, Topology of Cosmic Domains and Strings, *J. Phys. A* **9**, 1387 (1976).
- [2] A. Vilenkin, Cosmic strings and domain walls, *Physics reports* **121**, 263 (1985).
- [3] S. Sarangi and S. H. H. Tye, Cosmic string production towards the end of brane inflation, *Phys. Lett. B* **536**, 185 (2002), [arXiv:hep-th/0204074](#).
- [4] S. W. Hawking and S. F. Ross, Pair production of black holes on cosmic strings, *Physical review letters* **75**, 3382 (1995).
- [5] D. M. Eardley, G. T. Horowitz, D. A. Kastor, and J. Traschen, Breaking cosmic strings without monopoles, *Physical review letters* **75**, 3390 (1995).
- [6] D. Garfinkle and A. Strominger, Semiclassical wheeler wormhole production, *Physics Letters B* **256**, 146 (1991).
- [7] S. W. Hawking, G. T. Horowitz, and S. F. Ross, Entropy, area, and black hole pairs, *Physical Review D* **51**, 4302 (1995).
- [8] F. Dowker, J. P. Gauntlett, S. B. Giddings, and G. T. Horowitz, Pair creation of extremal black holes and kaluza-klein monopoles, *Physical Review D* **50**, 2662 (1994).
- [9] F. Mellor and I. Moss, Black holes and quantum wormholes, *Physics Letters B* **222**, 361 (1989).
- [10] R. B. Mann and S. F. Ross, Cosmological production of charged black hole pairs, *Physical Review D* **52**, 2254 (1995).
- [11] O. J. Dias and J. P. Lemos, Pair creation of de sitter black holes on a cosmic string background, *Physical Review D* **69**, 084006 (2004).
- [12] A. Ashoorioon and R. B. Mann, Black Holes as Beads on Cosmic Strings, *Class. Quant. Grav.* **31**, 225009 (2014), [arXiv:1402.2072 \[hep-th\]](#).
- [13] A. Ashoorioon and M. B. Jahani Poshteh, Black hole pair production on cosmic strings in the presence of a background magnetic field, *Physics Letters B* **816**, 136224 (2021).
- [14] A. Vilenkin, Y. Levin, and A. Gruzinov, Cosmic strings and primordial black holes, *Journal of Cosmology and Astroparticle Physics* **2018** (11), 008.
- [15] S. Clesse and J. García-Bellido, The clustering of massive Primordial Black Holes as Dark Matter: measuring their mass distribution with Advanced LIGO, *Phys. Dark Univ.* **15**, 142 (2017), [arXiv:1603.05234 \[astro-ph.CO\]](#).
- [16] A. Ashoorioon, A. Rostami, and J. T. Firouzjaee, EFT compatible PBHs: effective spawning of the seeds for primordial black holes during inflation, *JHEP* **07**, 087, [arXiv:1912.13326 \[astro-ph.CO\]](#).
- [17] H. Deng, J. Garriga, and A. Vilenkin, Primordial black hole and wormhole formation by domain walls, *JCAP* **04**, 050, [arXiv:1612.03753 \[gr-qc\]](#).
- [18] A. Ashoorioon, A. Rostami, and J. T. Firouzjaee, Examining the end of inflation with primordial black holes mass distribution and gravitational waves, *Phys. Rev. D* **103**, 123512 (2021), [arXiv:2012.02817 \[astro-ph.CO\]](#).
- [19] M. R. Morris, J.-H. Zhao, and W. Goss, A nonthermal radio filament connected to the galactic black hole?, *The Astrophysical Journal Letters* **850**, L23 (2017).
- [20] M. Astorino, Thermodynamics of Regular Accelerating Black Holes, *Phys. Rev. D* **95**, 064007 (2017), [arXiv:1612.04387 \[gr-qc\]](#).
- [21] M. Appels, R. Gregory, and D. Kubizňák, Thermodynamics of accelerating black holes, *Physical review letters* **117**, 131303 (2016).
- [22] A. Anabalón, M. Appels, R. Gregory, D. Kubizňák, R. B. Mann, and A. Övgün, Holographic thermodynamics of accelerating black holes, *Physical Review D* **98**, 104038 (2018).
- [23] N. Abbasvandi, W. Cong, D. Kubiznak, and R. B. Mann, Snapping swallowtails in accelerating black hole thermodynamics, *Class. Quant. Grav.* **36**, 104001 (2019), [arXiv:1812.00384 \[gr-qc\]](#).
- [24] N. Abbasvandi, W. Ahmed, W. Cong, D. Kubizňák, and R. B. Mann, Finely Split Phase Transitions of Rotating and Accelerating Black Holes, *Phys. Rev. D* **100**, 064027 (2019), [arXiv:1906.03379 \[gr-qc\]](#).
- [25] A. Anabalón, F. Gray, R. Gregory, D. Kubizňák, and R. B. Mann, Thermodynamics of charged, rotating, and accelerating black holes, *Journal of High Energy Physics* **2019**, 1 (2019).
- [26] M. Rostami, J. Sadeghi, S. Miraboutalebi, A. A. Mousadi, and B. Pourhassan, Charged accelerating AdS black hole of  $f(R)$  gravity and the Joule-Thomson expansion, *Int. J. Geom. Meth. Mod. Phys.* **17**, 2050136 (2020), [arXiv:1908.08410 \[gr-qc\]](#).
- [27] W. Ahmed, H. Z. Chen, E. Gesteau, R. Gregory, and A. Scoins, Conical Holographic Heat Engines, *Class. Quant. Grav.* **36**, 214001 (2019), [arXiv:1906.10289 \[hep-th\]](#).
- [28] S. Brenner, G. Giribet, and L. Montecchio, A closer glance at black hole pair creation, *arXiv preprint arXiv:2103.05782* (2021).
- [29] M. Zhang and R. B. Mann, Charged accelerating black hole in  $f(R)$  gravity, *Phys. Rev. D* **100**, 084061 (2019), [arXiv:1908.05118 \[hep-th\]](#).
- [30] M. Astorino and A. Viganò, Many accelerating distorted black holes, (2021), [arXiv:2106.02058 \[gr-qc\]](#).
- [31] Y.-K. Lim, Null geodesics in the c metric with a cosmological constant, *Physical Review D* **103**, 024007 (2021).
- [32] T. C. Frost and V. Perlick, Lightlike geodesics and gravitational lensing in the spacetime of an accelerating black hole, *Classical and Quantum Gravity* **38**, 085016 (2021).
- [33] A. Grenzebach, V. Perlick, and C. Lämmerzahl, Photon regions and shadows of accelerated black holes, *International Journal of Modern Physics D* **24**, 1542024 (2015).
- [34] M. Zhang and J. Jiang, Shadows of accelerating black holes, *Physical Review D* **103**, 025005 (2021).
- [35] C. Darwin, The Gravity Field of a Particle, *Proc. R. Soc. A* **249**, 180 (1959).
- [36] C. Darwin, The Gravity Field of a Particle. II, *Proc. R. Soc. A* **263**, 39 (1961).
- [37] K. S. Virbhadra and G. F. R. Ellis, Schwarzschild black hole lensing, *Phys. Rev. D* **62**, 084003 (2000).
- [38] K. S. Virbhadra, Relativistic images of Schwarzschild black hole lensing, *Phys. Rev. D* **79**, 083004 (2009).
- [39] M. Sasaki, T. Suyama, T. Tanaka, and S. Yokoyama, Primordial black holes—perspectives in gravitational wave astronomy, *Class. Quant. Grav.* **35**, 063001 (2018), [arXiv:1801.05235 \[astro-ph.CO\]](#).
- [40] B. J. Carr and M. Sakellariadou, Dynamical constraints on dark compact objects, *Astrophys. J.* **516**, 195 (1999).
- [41] W. Kinnersley and M. Walker, Uniformly accelerating

- charged mass in general relativity, *Physical Review D* **2**, 1359 (1970).
- [42] K. Hong and E. Teo, A new form of the c-metric, *Classical and Quantum Gravity* **20**, 3269 (2003).
- [43] J. Griffiths, P. Krtouš, and J. Podolský, Interpreting the c-metric, *Classical and Quantum Gravity* **23**, 6745 (2006).
- [44] J. Griffiths and J. Podolský, Accelerating and rotating black holes, *Classical and Quantum Gravity* **22**, 3467 (2005).
- [45] S. Weinberg, *Gravitation and cosmology: principles and applications of the general theory of relativity* (Wiley, 1972).
- [46] K. S. Virbhadra and G. F. R. Ellis, Schwarzschild black hole lensing, *Phys. Rev. D* **62**, 084003 (2000).
- [47] K. S. Virbhadra, D. Narasimha, and S. M. Chitre, Role of the scalar field in gravitational lensing, *Astron. Astrophys.* **337**, 1 (1998).
- [48] M. B. Jahani Poshteh and R. B. Mann, Gravitational lensing by black holes in einsteinian cubic gravity, *Physical Review D* **99**, 024035 (2019).
- [49] P. Kocherlakota *et al.* (Event Horizon Telescope), Constraints on black-hole charges with the 2017 EHT observations of M87\*, *Phys. Rev. D* **103**, 104047 (2021), [arXiv:2105.09343](https://arxiv.org/abs/2105.09343) [gr-qc].
- [50] K. Akiyama *et al.* (Event Horizon Telescope), First M87 Event Horizon Telescope Results. VI. The Shadow and Mass of the Central Black Hole, *Astrophys. J. Lett.* **875**, L6 (2019), [arXiv:1906.11243](https://arxiv.org/abs/1906.11243) [astro-ph.GA].
- [51] P. Schneider, J. Ehlers, and E. E. Falco, *Gravitational lenses* (Springer, 1992).
- [52] J. Synge, The escape of photons from gravitationally intense stars, *Monthly Notices of the Royal Astronomical Society* **131**, 463 (1966).
- [53] R. A. Hennigar, M. B. Jahani Poshteh, and R. B. Mann, Shadows, Signals, and Stability in Einsteinian Cubic Gravity, *Phys. Rev. D* **97**, 064041 (2018).
- [54] V. L. Fish, K. Akiyama, K. L. Bouman, A. A. Chael, M. D. Johnson, S. S. Doeleman, L. Blackburn, J. F. C. Wardle, and W. T. Freeman (Event Horizon Telescope), *Galaxies* **4**, 54 (2016).
- [55] K. Akiyama, K. Kuramochi, S. Ikeda, V. L. Fish, F. Tazaki, M. Honma, S. Doeleman, A. E. Broderick, J. Dexter, M. Mościbrodzka, , and K. L. Bouman, Imaging the Schwarzschild-radius-scale Structure of M87 with the Event Horizon Telescope Using Sparse Modeling, *JCAP* **838**, 1.
- [56] P. Kocherlakota, L. Rezzolla, H. Falcke, C. M. Fromm, M. Kramer, Y. Mizuno, A. Nathanail, H. Olivares, Z. Younsi, K. Akiyama, *et al.*, Constraints on black-hole charges with the 2017 eht observations of m87, *Physical Review D* **103**, 104047 (2021)